Journal of Inflammation Research

Dovepress
Taylor & Francis Group

Open Access Full Text Article

ORIGINAL RESEARCH

White Matter Anomaly Associated Cognitive Impairment During Systemic Inflammation Is Related to CX3CR1 Mediated Microglia-Node Interactions That Impacts the Conductive Function of Axons

Xue Shi[1], Jingdong Zhang[1–3], Huangying Zhao[3], Xinglong Yang[4], Feng Gao[1]

[1]Department of Anesthesiology and Pain Medicine, Hubei Key Laboratory of Geriatric Anesthesia and Perioperative Brain Health, and Wuhan Clinical Research Center for Geriatric Anesthesia, Tongji Hospital, Tongji Medical College, Huazhong University of Science and Technology, Wuhan, 430030, People's Republic of China; [2]The Key Laboratory of Molecular Biological Targeted Therapy of the Ministry of Education, and Hubei Key Laboratory of Biological Targeted Therapy, Huazhong University of Science and Technology, Wuhan, 430022, People's Republic of China; [3]Division of Pharmaceutical Science, University of Cincinnati College of Pharmacy, Cincinnati, OH, 45267, USA; [4]Core Facility of Research, The 5th Medical Center of PLA General Hospital, Beijing, 100071, People's Republic of China

Correspondence: Jingdong Zhang, The Key Laboratory of Molecular Biological Targeted Therapy of the Ministry of Education, Wuhan, 430022, People's Republic of China, Email jingdong_zhang@hotmail.com; Feng Gao, Department of Anesthesiology and Pain Medicine, Hubei Key Laboratory of Geriatric Anesthesia and Perioperative Brain Health, and Wuhan Clinical Research Center for Geriatric Anesthesia, Tongji Hospital, Tongji Medical College, Huazhong University of Science and Technology, Wuhan, 430030, People's Republic of China, Email fgao@tjh.tjmu.edu.cn

Background: The effects of CX3CR1 and CCR2 deficiency on cognition are related to microglia-neuron interactions and synaptic plasticity in the hippocampus. Contact between microglia and Ranvier's nodes has been identified in the brain white matter (WM). We propose that WM anomaly associated cognitive impairment during systemic inflammation is due to the alteration of microglia-node interactions, which impacts the conductive function of axons.

Methods: Novel object recognition and Y-maze tests were performed, and the corpus callosum (CC) axon compound action potential (CAP), microglia proportional area, density of microglia-node contact, and infiltrated circulating immune cells were examined in wild-type (WT), CX3CR1, and CCR2 knockout mice before and after systemic lipopolysaccharide (LPS) administration.

Results: CX3CR1 deficiency significantly reduced rate of exploring new objects and new paths, decreased CC CAP and microglia-node contact compared with WT mice. CX3CR1 or CCR2 knockout diminished the microglial proportional area. Systemic LPS significantly increased microglial proportional area and immune cell infiltration but decreased time and rate of exploring new objects and new paths, declined CAP, and reduced microglia-node contact in CX3CR1 expressed mice. The absence of CX3CR1 in normal conditions deteriorated cognitive performance and CC WM tract conductive function and reduced microglia density and microglia-node contact chance. However, defects in cognitive performance and CC WM tract conductivity, and disruption of microglia-node contact by systemic LPS were protected by CX3CR1 knockout.

Conclusion: CX3CR1 is involved in modulating CC WM microglia-node contact, maintaining the CC WM tract conductive function, and improving cognitive performance. In the context of systemic LPS and associated neuroinflammation, CX3CR1 seems to dominate the disruption of microglia-node communication and CC WM tract conductive function, consequently causing cognitive problem. This may be achieved primarily through CX3CR1 mediated microglia activities and activation and subordinately via the infiltration of $CX3CR1^{high}$ circulating immune cells into the CC WM tract.

Keywords: white matter tract, CX3CR1/CCR2 deficiency, microglia-node contact, axon compound action potential, cognitive performance, circulating immune cell infiltration

Received: 1 February 2025
Accepted: 16 June 2025
Published: 26 June 2025

Introduction

The relationship between neuroinflammation and cognitive impairment has been widely studied, and ample attention has been paid to pro-inflammatory cytokines and/or chemokines.[1,2] Generally, brain chemokines recruit circulating monocytes or macrophages into the brain or guide resident macrophages to migrate toward pathogens.[3,4] C-X3-C motif chemokine ligand 1 (CX3CL1) ie fractalkine, and C-C motif chemokine ligand 2 (CCL2) ie monocyte chemoattractant protein-1, play major chemotactic roles in the healthy brain and during neuroinflammation; however, their potential roles in cognitive performance have been overlooked.[5] Recently, it was shown that the CX3CL1-CX3CR1 axis plays an important role in cognitive function and dysfunction unrelated to its chemotactic task but is associated with hippocampal synaptic pruning through CX3CL1-CX3CR1 mediated microglia activity.[6–8] In addition, CCL2-CCR2 signaling mediates chronic pain-associated cognitive impairment by reducing hippocampal neurogenesis.[9]

White matter (WM) tracts bridge the connectivity of different functional groups of neurons and work in concert with gray matter to form a network capable of cognition.[10,11] The correlation between WM inflammation and defective cognition has been documented in various types of chronic systemic inflammation, *eg* as in obesity or asthma case,[12–14] and sepsis and/or systemic endotoxins.[15,16] In addition, aging-related cognitive decline is common and prevalent, a cause of which has been identified as implicit neuroinflammation that is considerably more severe in the WM tract.[17,18] Experimentally, we showed that both systemic lipopolysaccharide (LPS) and ex vivo LPS challenge impeded WM tract signal conduction;[19,20] however, the density of myelin basic protein was not changed by systemic LPS,[19] suggesting that demyelination does not occur in this acute neuroinflammation and is not always the cause of WM tract malfunction. As we have known, alterations of ion channels on Ranvier's node or of peri-node ion densities would affect WM tract conductivity.[21]

Recent studies have demonstrated the direct contact of microglial pseudopodia with Ranvier's node and/or node-like clusters of sodium channels in the corpus callosum (CC) and/or spinal cord WM tracts in rats, mice, and humans.[22–24] The density of these microglia-node contacts is changed by blocking a subclass of potassium channel.[23] Microglia are equipped with calcium ion sensors and calcium-activated potassium channels, and extracellular calcium concentration can modulate microglial pseudopodia extension.[25,26] Hence, microglia-node contact may play a role in monitoring peri-node electrolytic homeostasis and in maintaining proper excitability to sustain saltatory conduction. Because the CX3CL1-CX3CR1 axis is a key mediator of microglia-neuron interactions, it is rational to conjecture that overexpression or absence of CX3CR1 would deform microglia-node interactions as well. Furthermore, the number of microglia-node contacts is supposed to change in the presence of neuroinflammation due to deformation of microglia pseudopodia, which may affect the conductive function of the WM tract.

In the present study, we designed to use CX3CR1 or CCR2 knockout mice and their wild-type (WT) background strain to investigate and compare their cognitive capability and changes in cognitive capability following systemic LPS. We will also monitor functional alterations in the CC WM tract in WT, CX3CR1 and CCR2 deficiency mice by recording and analyzing the CC WM tract compound action potential (CAP) to determine whether this neurophysiological property is correlated with cognitive performance. Significantly, microglia-node contact in the CC WM will be counted and analyzed in normal or LPS-challenged WT, CX3CR1 and CCR2 deficiency mice, and we attempted to uncover any relationship between cognition performance, WM tract functional states, and density of microglia-node contacts. Considering the specific expression pattern of CX3CR1 or CCR2 in circulating immune cells,[3,4] we also plan to assess the extent of their infiltration into the CC WM by counting the infiltrated cells immunostained using a leukocyte common marker.

Materials and Methods

Animals

An equal number of male and female mice, aged 8–12 weeks, were used. Homozygous $CCR2^{+/+}CX3CR1^{-/-}$ and $CX3CR1^{+/+}CCR2^{-/-}$ were purchased from Cyagen Biosciences Suzhou Inc. (Taicang, Jiangsu, China) and homozygous littermates were obtained through cross-mating. The WT mice were C57BL/6J mice. All WT and transgenic mice were divided into behavior test, electrophysiological recording, and immunostaining groups with normal, saline-, and LPS-injected animals. Note, we performed electrophysiological recording after behavioral test for saline and LPS injection groups by using the same nest of mice. LPS was injected intraperitoneally (*i.p)*. at a dose of 1.5 mg/kg, once per day for 3 consecutive days. Equal volumes of sterile saline were injected in the same manner. All transgenic mice were viable and showed no obvious

developmental defects, consistent with previous reports.[27,28] Experimental protocols and animal care were carried out in accordance with the Huazhong University Research Council's Guide for the Care and Use of Laboratory Animals (matched with *European Union guideline for Laboratory Animal Care and Use*) and approved by the Institutional Research and Ethics Committee of the Tongji Medical College, Huazhong University of Science and Technology.

Reagents and Antibodies

LPS (*Escherichia coli*, L2880, Millipore-Sigma, Merck Shanghai LLC, Shanghai, China) was prepared in saline solution at 2 mg/mL and stored at −20°C before use. Polyclonal rabbit (Fujifilm Wako Guangzhou Trading Corp., Guangzhou, China) or goat (Abcam Shanghai Corp., Shanghai, China) anti-Iba-1 (ionizing calcium binding adaptor protein-1) were applied for immunostaining of microglia, monocytes or macrophages. Polyclonal rabbit anti-pan voltage-gated sodium channels (Pan Na^+v; Alomone Labs, Jerusalem, Israel) were used to visualize the Ranvier nodes and/or nodes like Na^+v cluster. Monoclonal rat anti-cluster of differentiation 45 (CD45; Clone 30-F11, Thermo-Fisher /Invitrogen Shanghai LLC, Shanghai, China) and polyclonal goat anti-CD45 (BD Biosciences, BD China, Suzhou, China) were used as leukocyte markers for infiltrating immune cells, including monocytes. Monoclonal mouse anti-myeloperoxidase (MPO; clone 266–6K1; Santa Cruz Asian distributor, Shanghai, China) was used to distinguish between infiltrating neutrophils and monocytes. All fluorescent dyes (Alexa Fluor 405, 488, and 594) conjugated with secondary antibodies (Thermo-Fisher/ Invitrogen, Shanghai) were used to visualize the primary labeling.

Novel Object Recognition Test (NORT)

Normal mice and saline- and LPS-injected littermates were trained and videoed for 10 min in a 45 × 45 × 45 cm^3. Saline- and LPS-injected mice were tested on the 2nd day after the final injection. Animals were placed in behavioral testing room about 2h for habituation of environment. During training, ie familiarization phase, each mouse explored in the field for 10 min with two identical objects (A1 and A2). The discrimination phase was performed an hour after familiarization. Each mouse was returned to the square space, where one of the familiar objects (A2) was replaced by a novel object (A3). In the discrimination phase, each mouse was allowed to explore the A1 and A3 objects for 10 min, and the animal's exploratory actions were recorded and analyzed. The time and number of exploring upon each object were documented, and discrimination index was calculated with both "[Time spending on A3 (novel object) / Time spending on both A1 (old) + A3] × 100%", and "[Number of exploring A3 (novel object) / Total number of exploring A1 (old) + A3] × 100%" was used to index the animal's tendency or capability to recognize a novel object.[29,30]

Y-Maze Test (YMT)

The Y-maze apparatus is composed of three 35 × 6 × 15 cm^3 arms, with 120° between, marked as A, B and C. Next day to the NORT, animals were placed in behavioral testing room about 2h for habituation of environment. Then, each mouse was placed at the center of the apparatus and allowed to explore the arms freely for 5 min. In the testing phase, each mouse was released at the terminal of arm A and was allowed to move freely into the other arm. In this study, the animals were only subjected to spontaneous alternative tasks[31,32] and their activities were subsequently videoed and analyzed. The correct activity is to keep entering a different arm and not return. The ratio of correct alternations was calculated as "[number of correct alternations/ (total correct + error alternations) – 2] × 100%",[31,32] which indexes the spatial cognitive capability.

CC WM Tract Electrophysiological Recording

On the day after the behavioral test, the saline- and LPS-injected littermates were euthanized with isoflurane and then decapitated. The brains were quickly dissected out of the cranial cavity, placed into a beaker containing ice-cold (4°C) oxygenated artificial cerebrospinal fluid (ACSF), and cut into 500 μm thick coronal slices containing the CC. They were then transferred to another beaker with oxygenated ACSF at room temperature and bathed for an hour before recording. The CC axons CAP was evoked by constant step-up current from 0.10 to 0.50 mA (0.05 mA/step, 40 μs duration, 0.2 Hz) via a bipolar tungsten stimulating electrode (with 0.95 mm inter-polar gap, 0.5 MΩ in Saline, World Precision Instruments China, Shanghai). The recording electrodes, made from borosilicate glass capillaries (1.5/0.84 OD/ID, WPI China, Shanghai) and filled with the same ACSF (impedance 1–4 MΩ), were placed 1.5 ~ 2.0 mm away from

the stimulating site. Signals were amplified using an Axopatch 1D amplifier (Molecular Devices, San Jose, CA, USA) and a Dagan EX4-400 amplifier (Dagan Corp., Minneapolis, MN, USA), filtered at 1kHz, digitized at 5kHz using a Digidata 1440A interface (Molecular Devices), and saved on a Dell computer equipped with pCLAMP 10.1 software (Molecular Devices). The recorded CAP was plotted as an input - output (I/O) curve that indexes the functional profile of the investigated WM tract.

Immunofluorescent Staining

On the day after the behavioral test, animals in the saline and LPS injection groups were euthanized with an overdose of sodium pentobarbital (80–100 mg/kg) and transcardially perfused with cold saline, followed by 10% formalin phosphate (Fisher Chemicals, pH 7.2–7.4). The brains were removed, post-fixed overnight, and cryoprotected with 30% sucrose in phosphate-buffered saline (PBS; pH 7.2–7.4). Frozen coronal sections (14 μm) were cut, mounted on plus-coated slides, and stored at −80°C. During staining, a control section on each slide was isolated using Super PAP Pen, for which all procedures were the same except that the primary antibody was omitted. Sections were incubated in goat anti-Iba-1 (1:200–500) combined with either rabbit anti-Pan Na^+v (1:100–200) or rat anti-CD45 (1:100–200) overnight. A combination of rabbit anti-Iba-1 (1:500) and goat anti-CD45 (1:20 ~ 50) was also used. Some sections were double-immunostained with rat anti-CD45 and mouse anti-MPO antibodies (1:500). Alexa Fluor 488 or 594 (1:1000) was used to visualize primary staining.

Quantification of Immunofluorescent Stained Structures in 20X Images of CC WM

1) Proportional Iba-1 positive areas were processed using Photoshop and measured using the ImageJ software. Iba-1 labeled areas were converted to grayscale images by Photoshop, and a threshold was set up in ImageJ and "Analyze Particles" function was used to measure the Iba-1 positive areas. The entire CC area, excluding the adjacent gray matter and lateral ventricles, was also measured. The proportional area was the Iba-1 positive area divided by the entire CC area.[33]
2) The density or intensity of the Pan Na^+v positive dots was indexed by intensity/area and measured using Slidebook 6 (Intelligent Imaging Innovations Inc., Denver, CO, USA). Anti-Pan Na^+ v-labeled dots in an identified CC area (excluding gray matter and lateral ventricle) were adjusted to be seen distinctly and masked. The intensity per μm^2 of each masked spot was measured.
3) Confocal microscopy was used to verify the contact between Iba-1 and Pan Na^+v labeling. The Nikon A1 confocal microscope (Nikon, Japan) was driven by the BioRad Laser Sharp 2000 imaging program (Digital BioRad Center, Pleasanton, CA, USA). Alexa Fluor 594 labeling was viewed through a 561 excitation laser line with 10 nm resolution of the spectra. Alexa Fluor 488 was visualized using a 488 excitation laser line through 10 nm spectra. The focal plane and/or z-stack layer was 2 μm thick during the laser scanning.
4) Contact between Iba-1 labeled pseudopodia and Pan Na^+v positive dots was counted on every other five sections containing the CC using Photoshop (Adobe Systems Inc., San Jose, CA) and "Multipoint Function" of ImageJ (NIH, Bethesda, MD, USA). The number of contacts or immediate appositions was normalized by the CC area, which was finally converted from pixels to square millimeters (mm^2).
5) Number of CD45 labeled cells was counted in every other five sections, with Photoshop and "Multipoint Function" of ImageJ, and normalized by the whole measured CC area, as previously mentioned.

Statistics Analysis

Behavioral test data of WT, $CCR2^{+/+}CX3CR1^{-/-}$ and $CX3CR1^{+/+}CCR2^{-/-}$ mice were processed using one-way analysis of variance (ANOVA) with both Tukey's and Newman-Kaul's post-hoc tests for sure the consistence. Data from saline- and LPS-injected littermates were verified using Student's *t*-test. One-way ANOVA of the area under the curve (AUC) was used to relate the differences in I/O curves plotted from CAP recorded in saline- and LPS-injected mice. Individual AUC value was calculated by using Excel Trapezoidal Rule; thus, the basic formula is (x2-x1) × (y2+y1)/2 in which the "y" represents CAP amplitude and the "x" stands for increment of stimulation currents. Student's *t*-test was used to compare CAP in response to each stimulation intensity. The Iba-1 positive proportional areas, microglia-node contacts, and positive CD45 cells in the CC were analyzed using one-way ANOVA with both Tukey's and Newman-Kaul's post-test for comparison

between the saline and LPS injection groups. Statistical analyses were performed using Graph Pad Prism 5 (Graph Pad Software Inc. La Jolla, CA), and the marks of "*" and "**" represent $p < 0.05$ and $p < 0.01$, respectively.

Results

Novel Object Recognition and Y Maze Tests

1) Observations in normal mice: Neither CCR2 nor CX3CR1 knockout evidently impeded the activity of mice exploring assigned objects (A1 and A2) during the familiarization phase. The time spending (second) on the new object (A3) vs total time on both objects (A1+ A3) was not significantly different among WT and two transgenic mice (Figure 1Ai); while, the rate of exploring novel (A3) vs total objects (A1 + A3) was significantly decreased by knockout of CX3CR1 (Figure 1Bi, $F_{2, 40} = 11.01$, $p < 0.05$, n = 9). The ratio of correct alternation during the Y-maze test was nearly-significantly reduced (Figure 1Ci, $F_{2, 39} = 2.89$, $p = 0.0673$, n = 8) by CX3CR1 knockout compared to that in WT mice (n = 5), reflecting that CX3CR1 knockout undermined the ability of animals, to a considerable extent, to recognize novel objects and explore new paths.
2) Effect of systemic LPS on object recognition behavior: The total activities of exploration of the assigned object (A1 and A2) during the familiarization phase was evidently decreased by LPS treatment in all WT and transgenic mice probably due to slowness of locomotion. In contrast, the time and rate of exploring novel objects (A3) vs total objects (A1 + A3) in the discrimination phase was significantly decreased by LPS treatment in WT (Figure 1Aii, $F_{6, 86} = 11.02$, $p < 0.01$; Figure 1Bii, $F_{5, 76} = 12.21$, $p < 0.05$, n = 8) and $CX3CR1^{+/+}CCR2^{-/-}$ mice (Figure 1Aii, $F_{6, 86} = 11.02$, $p < 0.05$: Figure 1Bii, $F_{5, 76} = 12.21$, $p < 0.05$, n = 8), but not in $CCR2^{+/+}CX3CR1^{-/-}$ mice (n = 9).
3) Effect of Systemic LPS on spatial cognition in the Y-maze: Systemic LPS clearly impaired spatial cognition in both WT and $CX3CR1^{+/+}CCR2^{-/-}$ mice, as indicated by a significant reduction in the correct alternation ratio in WT (Figure 1Cii, $F_{5, 75} = 7.89$, $p < 0.05$, n = 8) and $CX3CR1^{+/+}CCR2^{-/-}$ mice (Figure 1Cii, $F_{5, 75} = 7.89$, $p < 0.05$, n = 8), but not in $CCR2^{+/+}CX3CR1^{-/-}$ mice (n = 9).

Changes of CC MW Tract CAP Plotted Input-Output Curves

The I/O response curves plotted from the CAP of the CC fibers were shown in Figure 2. CAP amplitudes were measured and analyzed based on previous studies.[19,34,35] Accordingly, CAP commonly consists of two components: a high-amplitude and short-latency component N1, and a small waveform with longer latency N2 (Figure 2A). The former represents CAP of myelinated nerve fibers and the latter signifies the recording from unmyelinated axons.[34,35]

1) Comparison of the N1 part of CAP among WT, $CX3CR1^{+/+}CCR2^{-/-}$ and $CCR2^{+/+}CX3CR1^{-/-}$mice: A statistical comparison of I/O curves from the N1 part of CAP between normal WT and $CX3CR1^{+/+}CCR2^{-/-}$ mice showed no significant differences (Figure 2B, n = 8). Assessment of areas under the N1 I/O curves in normal WT and $CCR2^{+/+}CX3CR1^{-/-}$ mice exhibited a visible difference (Figure 2C, $F_{8, 108} = 70.27$, n = 7) between their AUC, *T*-test of CAP amplitude at 0.40 and 0.45 mA stimulation showed a significantly lower CAP in CX3CR1 deficiency mice than in WT mice (Figure 2C, $p < 0.05$ at both points, t = 3.28, t = 4.17, df = 13, n = 7).
2) Effects of systemic LPS on N1 CAP in WT, $CX3CR1^{+/+}CCR2^{-/-}$ and $CCR2^{+/+}CX3CR1^{-/-}$mice: Analysis of areas under the N1 I/O curves revealed that systemic LPS significantly downshifted the curve recorded from the CC of WT mice (see Supplementary Figure 1A), which is consistent with previous research, including ours.[19,20,36] The areas under the N1 curves of $CX3CR1^{+/+}CCR2^{-/-}$ mice displayed a nearly significant downshift of I/O curves following LPS treatment (Figure 2D, $F_{8, 153} = 60.37$, $p = 0.0787$, n = 8), with a significant reduction in CAP amplitude at 0.40 ~ 0.50 mA stimulation points, compared to the saline littermates (2D, $p < 0.01$ at 0.40 and 0.45 mA points, t = 3.51, t = 3.06, df = 15; $p < 0.05$ at 0.05 mA point, t = 4.03, df = 15, n = 8). The areas under the N1 curves of $CCR2^{+/+}CX3CR1^{-/-}$ mice showed no obvious differences between the saline- and LPS-injected mice (Figure 2E, n = 7).

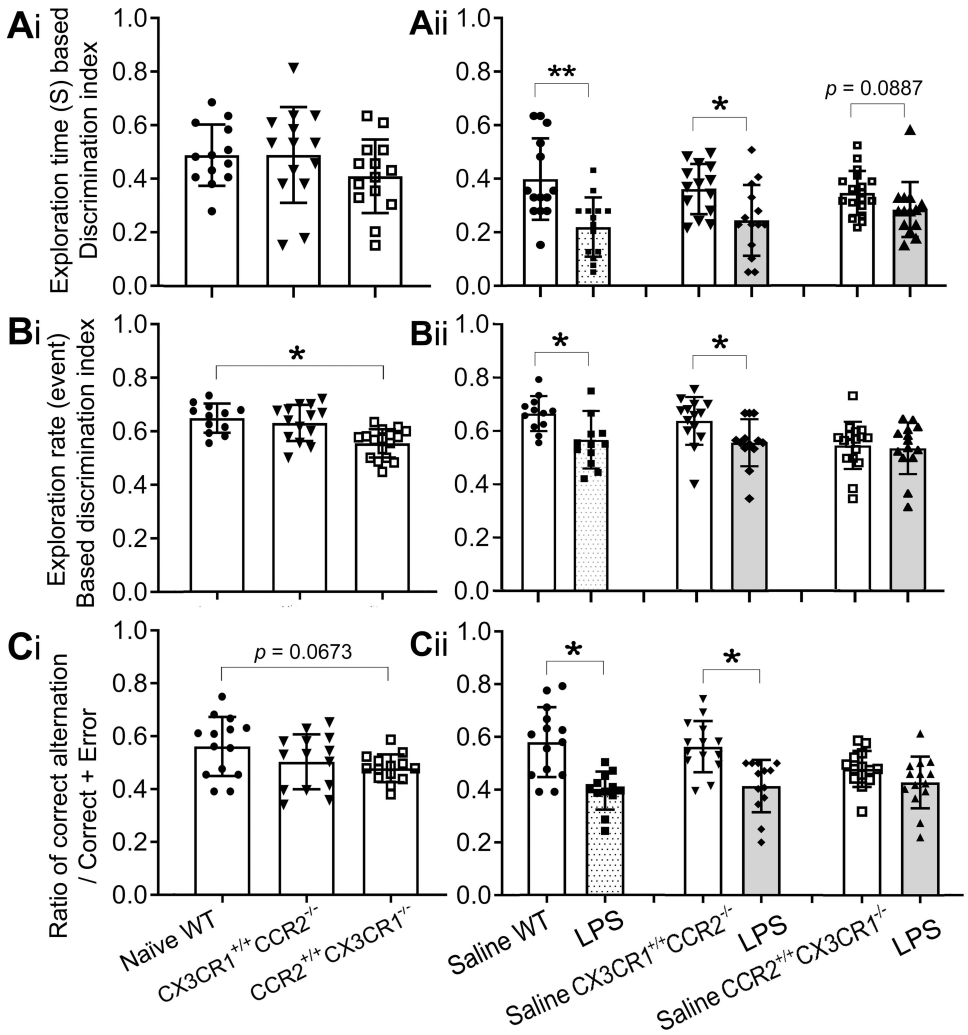

Figure 1 Cognitive behavior test in normal, saline and LPS injected WT, CX3CR1 or CCR2 deficiency mice. (**A**i) the ratio of time on exploring novel object vs total exploration time during NORT appeared not evidently difference among naïve WT and two normal transgenic mice. (**A**ii) however, that ratio of exploration time upon novel object vs total exploration time was significantly decreased by LPS treatment in WT ($F_{6, 86}$ = 11.02, $p < 0.01$, n = 8) and $CX3CR1^{+/+}CCR2^{-/-}$ ($F_{6, 86}$ = 11.02, $p < 0.05$, n = 8) mice, and was lowered down by LPS treatment towards a significant level in $CCR2^{+/+}CX3CR1^{-/-}$ ones ($p = 0.0887$, n = 9). (**B**i) while, the ratio of exploration events on novel object vs total exploration rate during NORT was significantly higher in naïve WT ($F_{2, 40}$ = 11.01, $p < 0.05$, n = 9) than that in normal $CCR2^{+/+}CX3CR1^{-/-}$ mice. (**B**ii) that ratio of exploration rate upon novel object vs total exploration rate was significantly decreased by LPS treatment in WT ($F_{5, 76}$ = 12.21, $p < 0.05$, n = 8) and $CX3CR1^{+/+}CCR2^{-/-}$ ($F_{5, 76}$ = 12.21, $p < 0.05$, n = 8) mice, but not in $CCR2^{+/+}CX3CR1^{-/-}$ ones (n = 9). (**C**i) the ratio of correct alternation during YMT in naïve WT mice was nearly significant higher ($F_{2, 39}$ = 2.89, $p = 0.0673$, n = 8) than that in $CCR2^{+/+}CX3CR1^{-/-}$ mice. (**C**ii) LPS challenge significantly reduced the ratio of correct alternation in WT ($F_{5, 75}$ = 7.89, $p < 0.05$, n = 8) and $CX3CR1^{+/+}CCR2^{-/-}$ ($F_{5, 75}$ = 7.89, $p < 0.05$, n = 8) nice, but not in $CCR2^{+/+}CX3CR1^{-/-}$ mice (n = 9). The marks of "*" and "**" represent $p < 0.05$ and $p < 0.01$, respectively.

3) Comparing the N2 waveform recorded from unmyelinated CC fibers between naïve WT and $CX3CR1^{+/+}CCR2^{-/-}$ or $CCR2^{+/+}CX3CR1^{-/-}$ mice showed no evident differences (Figure 2F and G, n = 7 respectively).
4) Effects of systemic LPS on N2 part of CAP: The areas under N2 curves of the WT mice was evidently down-shifted by systemic LPS (see Supplementary Figure 1B), which was in accordance with our previous observations.[19,20] Comparison of areas under N2 curves of saline- and LPS-injected $CX3CR1^{+/+}CCR2^{-/-}$ littermates showed an observable downshift of the curve (Figure 2H, $F_{8, 153}$ = 60.35, $p = 0.0974$, n = 8) by LPS with a significant decline in N2 CAP at the 0.50 mA stimulation point (2H, $p < 0.05$, t = 5.01, df = 15, n = 8). In $CCR2^{+/+}CX3CR1^{-/-}$ mice, the N2 curves showed no clear difference between saline- and LPS-injected cases (Figure 2I, n = 8).

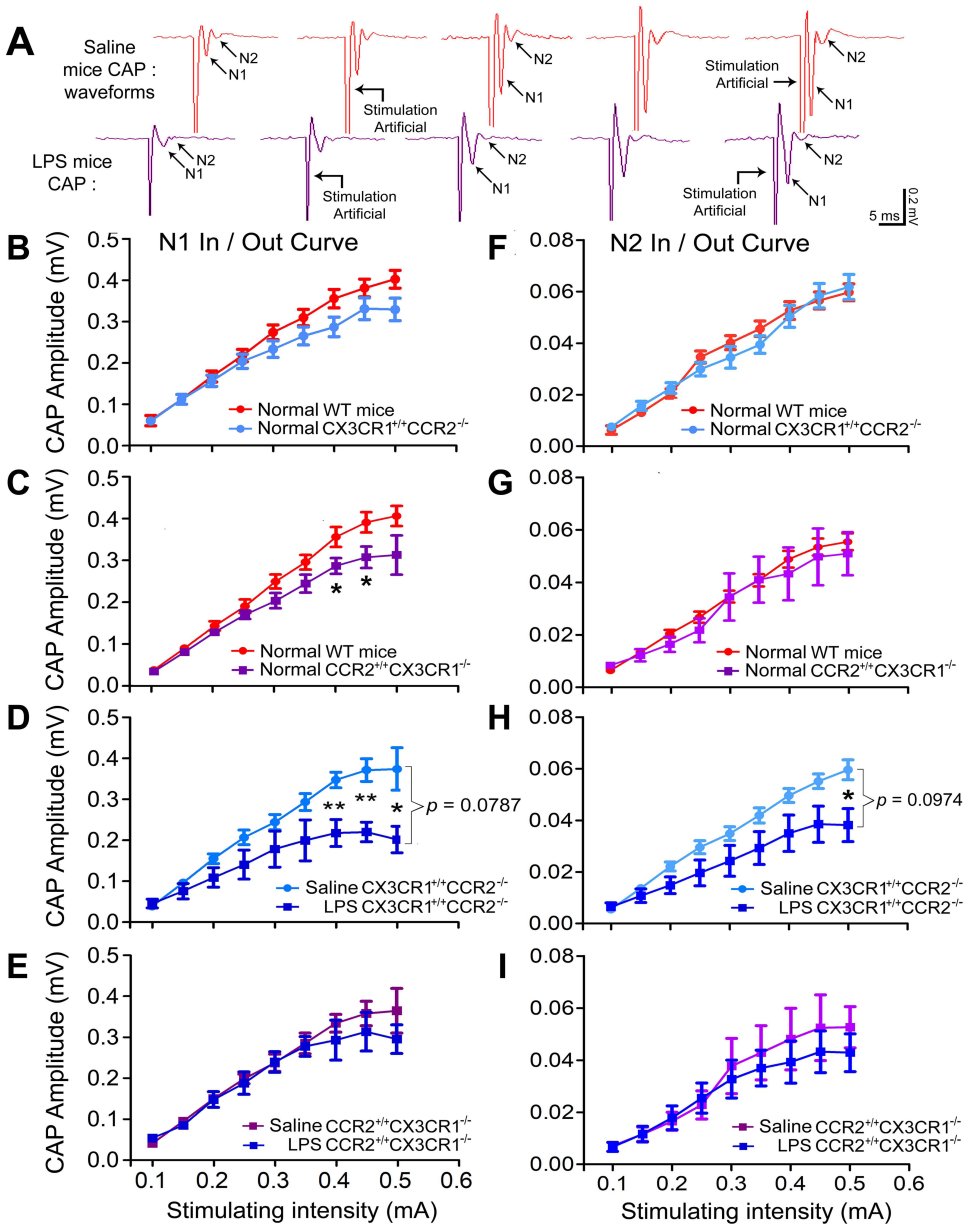

Figure 2 I/O curves from CAP recorded on the CC of normal, saline and LPS injected mice. (**A**) CAP classification shown by representative N1 and N2 waveforms that recorded from the CC WM tract of saline and LPS treated WT mice. (**B**) areas under N1 I/O curve of normal WT (n = 3) and CX3CR1$^{+/+}$CCR2$^{-/-}$ (n =5) mice showed no evident difference. (**C**) areas under N1 I/O curve of CCR2$^{+/+}$ CX3CR1$^{-/-}$ mice (n = 4) was visibly down-shifted in comparison that in WT mice ($F_{8,\ 108}$ = 70.27, n = 3), with significantly declined CAP amplitude at 0.40 and 0.45 mA stimulation points ($p < 0.05$ at both points, t = 3.28, t = 4.17, *df* = 13). (**D**) systemic LPS nearly significantly down-shifted N1 I/O curve in CX3CR1$^{+/+}$CCR2$^{-/-}$ mice ($F_{8,\ 153}$ = 60.37, $p = 0.0787$, n = 8) with significant declination of CAP amplitude in response to 0.40 ~ 0.50 mA stimulations ($p < 0.01$ at 0.40 and 0.45 mA points, t = 3.51, t = 3.06, *df* = 15; $p < 0.05$ at 0.50 mA stimulation, t = 4.03, *df* = 15), in comparison of saline injected littermates. (**E**) LPS treatment did not evidently change the N1 I/O curve in CCR2$^{+/+}$CX3CR1$^{-/-}$ mice (n = 7). (**F** and **G**), no obvious difference of N2 I/O curves was detected between WT (n = 3) and either receptor deleted mice (n = 4, respectively). (**H**) LPS challenge markedly down-shifted the N2 I/O curve of CX3CR1$^{+/+}$CCR2$^{-/-}$ mice ($F_{8,\ 153}$ = 60.35, $p = 0.0974$, n = 8), with a significant reduction of CAP amplitude at 0.50 mA stimulation point ($p < 0.05$, t = 5.01, *df* = 15) in comparison of saline injected littermates. (**I**) no evident difference of N2 I/O curve was observed between saline and LPS injected CCR2$^{+/+}$CX3CR1$^{-/-}$ mice (n = 8). The marks of "*" and "**" represent $p < 0.05$ and $p < 0.01$, respectively.

Iba-1 Positive Proportional Area and CC Microglia Activation

1) Microglial proportional area in the CC of normal WT, CX3CR1$^{+/+}$CCR2$^{-/-}$and CCR2$^{+/+}$CX3CR1$^{-/-}$ mice: resting microglia in WT and transgenic mice showed fine somata with delicate pseudopodia (Figure 3A, C and E; frame areas: (Figure 3G, J and M), without detectable morphological differences. The CC Iba-1 positive proportional

https://doi.org/10.2147/JIR.S513429

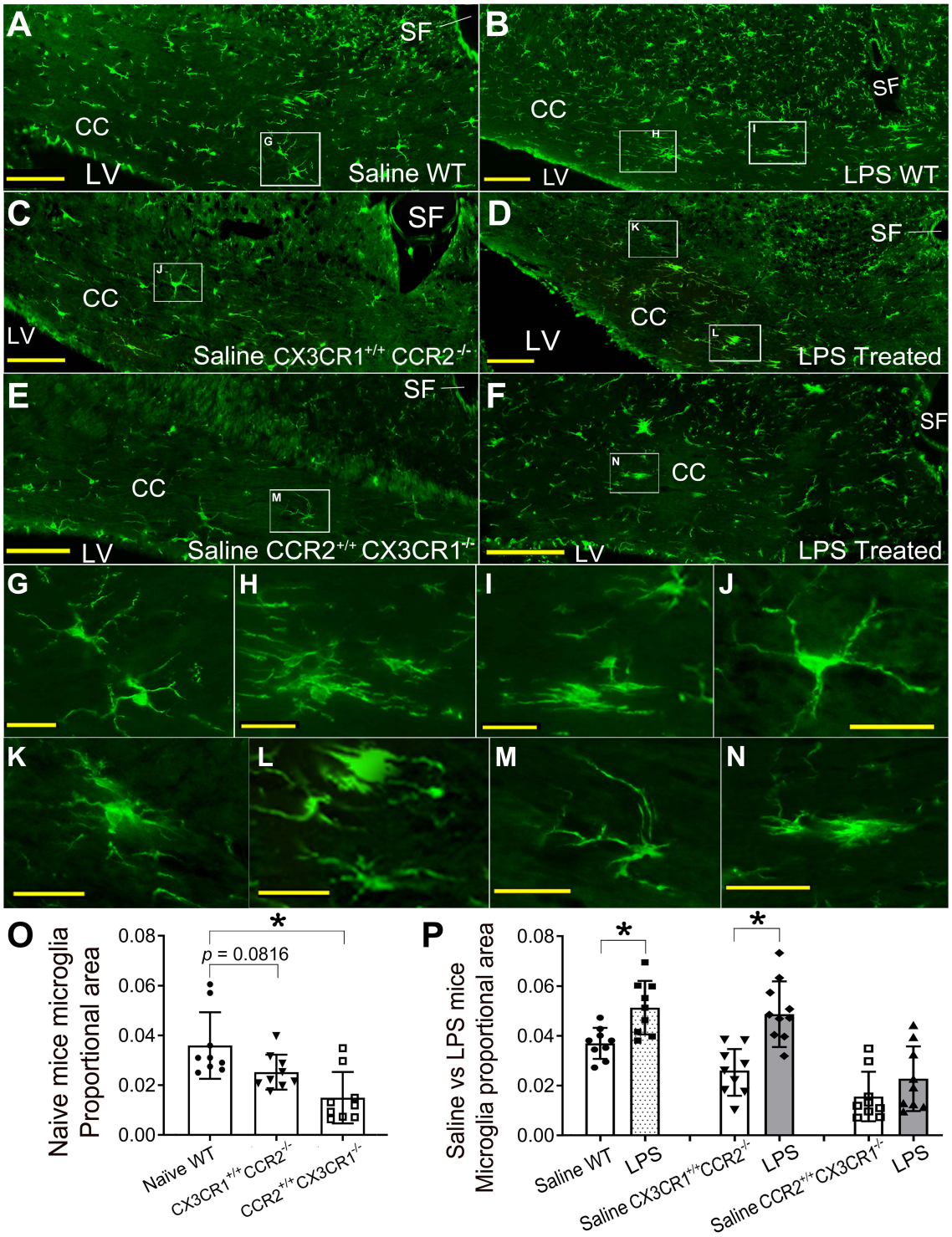

Figure 3 Resting and activated microglia in the CC of WT, CX3CR1$^{+/+}$CCR2$^{-/-}$ and CCR2$^{+/+}$CX3CR1$^{-/-}$ mice. (**A, C** and **E**) resting microglia in normal WT, CX3CR1$^{+/+}$CCR2$^{-/-}$ and CCR2$^{+/+}$CX3CR1$^{-/-}$ mice. (**B, D** and **F**) activated microglia in WT and two transgenic mice following systemic LPS. (**G, J** and **M**) higher magnification of frame areas in (**A, C** and **E**) showing fine soma with delicate pseudopodia of resting microglia. (**H, I, K, L** and **N**) frame areas from (**B, D** and **F**) displaying activated microglia with hypertrophic soma, hyper-ramified pseudopodia and amoeba like (**I, L**, and **N**) morphology evoked by LPS challenging. (**O**), the CC microglial proportional area in naïve WT mice (n = 3) was evidently larger than that in normal CX3CR1$^{+/+}$CCR2$^{-/-}$ mice ($F_{2, 24}$ = 8.86, p = 0.0816, n = 3), and significantly bigger than that in CCR2$^{+/+}$CX3CR1$^{-/-}$ mice ($F_{2, 24}$ = 8.86, $p < 0.05$, n = 4). (**P**) systemic LPS significantly increased the CC microglial proportional area in WT ($F_{6, 48}$ = 15.13, $p < 0.05$, n = 3) and CX3CR1$^{+/+}$CCR2$^{-/-}$ ($F_{6, 48}$ = 15.13, $p < 0.05$, n = 3) mice, but not in CCR2$^{+/+}$CX3CR1$^{-/-}$ mice (n = 4), in comparison of their saline injected littermates. The mark of "*" represents $p < 0.05$. LV, lateral ventricle. SF, sagittal fissure. Scale bars are 100 μm in (**A**–**F**), and are 25 μm in (**G**–**N**).

areas were obviously reduced by CCR2 knockout (Figure 3O, $F_{2,\ 24} = 8.86$, $p = 0.0816$, n = 3) and significantly decreased by CX3CR1 knockout (Figure 3O, $F_{2,\ 24} = 8.86$, $p < 0.05$, n = 4), compared to WT mice (n = 3).

2) Following systemic LPS, the CC microglia in all WT and transgenic mice were activated, as reflected by a large number of hypertrophic microglia and/or hyper-ramified pseudopodia (Figure 3B, D and F, and frame areas: Figure 3H, I, K, L and N), with some amoeba-like cells in between (I, L, and N). Systemic LPS significantly increased the proportional area in the CC of WT (Figure 3P, $F_{6,\ 48} = 15.13$, $p < 0.05$, n = 3) and $CX3CR1^{+/+}CCR2^{-/-}$mice (Figure 3P, $F_{6,\ 48} = 15.13$, $p < 0.05$, n = 3), and visibly enlarged that in $CCR2^{+/+}CX3CR1^{-/-}$ mice (n = 4), compared to that in saline-injected littermates.

Pan Na^+v Labeling Intensity and Microglia-Node Contact in the CC

1) Intensity of Pan Na^+v labeling in the CC: Anti-Pan Na^+v labeled Ranvier's nodes and node-like spots were about 0.2 ~ 1.0 μm in size and densely distributed in the CC (Figures 4, 5 and Supplementary Figure 2). There was no clear difference in the intensity of Pan Na^+v labeling between the normal CC of WT and the two transgenic mice (Figure 4E). Systemic LPS did not significantly alter the intensity of Pan Na^+v labeling in the CC of WT and transgenic mice (Figure 4B, D and F; Supplementary Figure 2).
2) Quantification of contacts or close appositions between Iba-1 and Pan Na^+v labeling: A number of Iba-1 labeled pseudopodia were observed to be closely apposite upon Pan Na^+v labeled dots (or nodes) in the CC of normal WT (Figure 4A, C and E, frame areas and insets a1 – a3), $CX3CR1^{+/+}CCR2^{-/-}$ (Figure 5A and E, insets a1 – a3), and $CCR2^{+/+}CX3CR1^{-/-}$ (Figure 4E; Figure 5C and G, insets c1 – c3) mice. The number of close appositions between Iba-1 and Pan Na^+v labeling in WT mice (n = 3) was significantly higher than that in $CCR2^{+/+}CX3CR1^{-/-}$ mice (Figure 4G, $F_{2,\ 51} = 12.02$, $p < 0.05$, n = 4).
3) Following systemic LPS administration, the number of close appositions between Iba-1 and Pan Na^+v labeling in the CC was significantly reduced in WT mice (Figure 4B and D, insets b1 and b2; Figure 4H, $F_{6,\ 113} = 25.39$, $p < 0.05$, n = 3) and $CX3CR1^{+/+}CCR2^{-/-}$ (Figure 5B and F, insets b1 and b2; Figure 4H, $F_{6,\ 113} = 25.39$, $p < 0.05$, n = 4), but not in $CCR2^{+/+}CX3CR1^{-/-}$ mice (Figure 5D and H, insets d1 and d2; Figure 4H, n = 5).
4) Confocal microscopic verification: Contact of Iba-1 labeled process upon Pan Na^+v positive dot (solid arrow) was verified through confocal microscopic observation (Figure 4C and D; Figure 5E–G). Close apposition between the two labeling (empty arrow), commonly with 0.5 ~ 1.5 μm gap, was also visualized from time to time (Figure 4C and D; Figure 5E, G and H).

Count and Analysis of Anti-CD45 Labeled – Infiltrated Circulating Immune Cells in the CC

1) Majority of CD45 labeled cells were ovoid-shaped, devoid of pseudopodia, and 15–20 μm in diameter along the long axis (Figure 6A, C, E, G and I, arrows and insets). Some were round with diameters of approximately 10 μm or smaller (arrows in Figure 6A, C, E and I). Cell-like MPO labeling was not observed (Figure 6; Supplementary Figure 3) namely, no neutrophil infiltrated in the CC. Statistically, the absence of CX3CR1 (n = 4) resulted in significant fewer CD45 positive cells compared to that in WT (n = 3) mice (Figure 6C and I; K, $F_{2,\ 24} = 7.92$, $p < 0.01$). The CCR2 deficiency led to an obvious variant number of CD45 labeled cells but not at a significant level (Figure 6A, C, E, G and K).
2) Following systemic LPS administration, the size of the CD45 positive infiltrating immune cells appeared rather hypertrophic (Figure 6B, D, F, H, and J, frame areas, and insets). Sometimes, CD45 labeled cells were clustered in WT (Figure 6D, paired arrows) and $CX3CR1^{+/+}CCR2^{-/-}$ mice (6F, paired arrows) but not in $CCR2^{+/+}CX3CR1^{-/-}$ mice. A few ramified CD45 positive cells were observed in the CC of LPS-treated $CCR2^{+/+}CX3CR1^{-/-}$ mice (Figure 6J, inset). Some changes in anti-MPO (neutrophil) labeling was described in Supplementary File. Statistically, the number of CD45 positive cells in the CC was significantly increased by LPS challenge in WT (n = 3) and $CX3CR1^{+/+}CCR2^{-/-}$ mice (Figure 6L, $F_{7,\ 62} = 32.10$, $p < 0.05$ for both, n = 4), but not in $CCR2^{+/+}CX3CR1^{-/-}$ mice (n = 4), compared to their saline-injected littermates. Observation of anti-MPO labeled structures in the CC (see Supplementary Files).

https://doi.org/10.2147/JIR.S513429

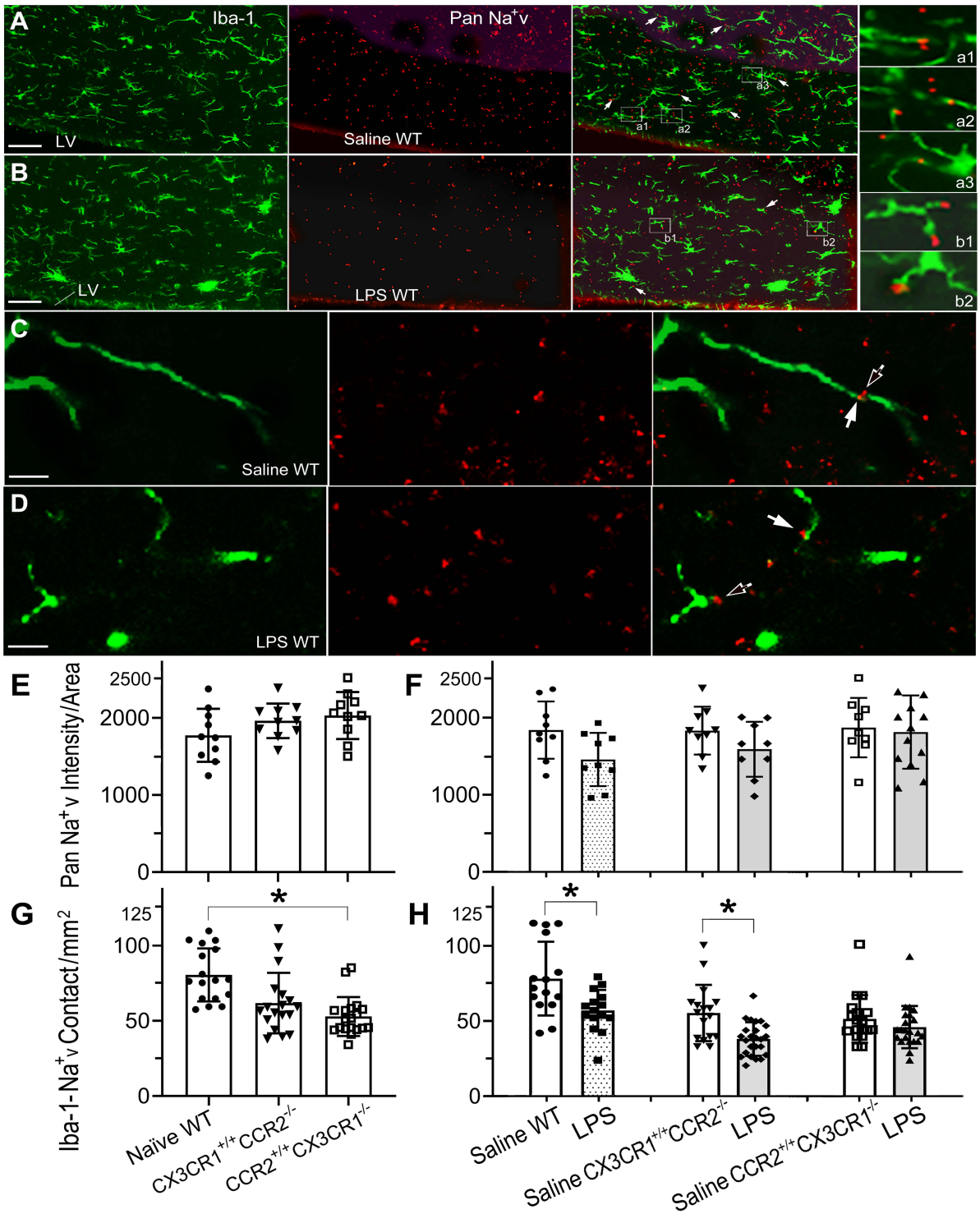

Figure 4 Contact of Iba-1 labeled pseudopodia upon Pan Na^+v positive dot in the CC of WT mice. (**A** and **B**) identification of contacts between Iba-1 and Pan Na^+v labeling (arrows and frame areas) in the CC of saline and LPS injected WT mice. (a1–a3) (**b1** and b2) magnified images from the frame areas in (**A** and **B**) (**C** and **D**) confocal microscopic verification of contact (solid arrows) or close apposition (empty arrows), commonly with 0.5 −1.5 μm cleft, between Iba-1 labeled pseudopodia and Pan Na^+v positive dot. (**E**) Pan Na^+v density among naïve WT and two normal transgenic mice, which appeared to be no clear difference of that density among naïve WT and two normal transgenic mice. (**F**) further, systemic LPS challenge seemed not significantly change the densities of these Pan Na^+v labeling. (**G**) while, CX3CR1 knockout (n = 4) significantly reduced the number of contact or close apposite between Iba-1 labeled pseudopodia and Pan Na^+v positive dots ($F_{2,\ 51} = 12.02$, $p < 0.05$, WT) compared to WT ones (n = 3). (**H**) LPS challenge significantly decreased the contact or close apposition between microglia pseudopodia and Pan Na^+v positive dots in the CC of WT (n = 3) and $CX3CR1^{+/+}CCR2^{-/-}$ mice ($F_{6,\ 113} = 25.39$, $p < 0.05$ for both, n = 4), but not in $CCR2^{+/+}CX3CR1^{-/-}$ mice (n = 5), in comparison of their saline injected littermates. The mark "*" represents $p < 0.05$. LV: lateral ventricles. Scale bars are 20 μm in (**A** and **B**) and 5 μm at (**C** and **D**).

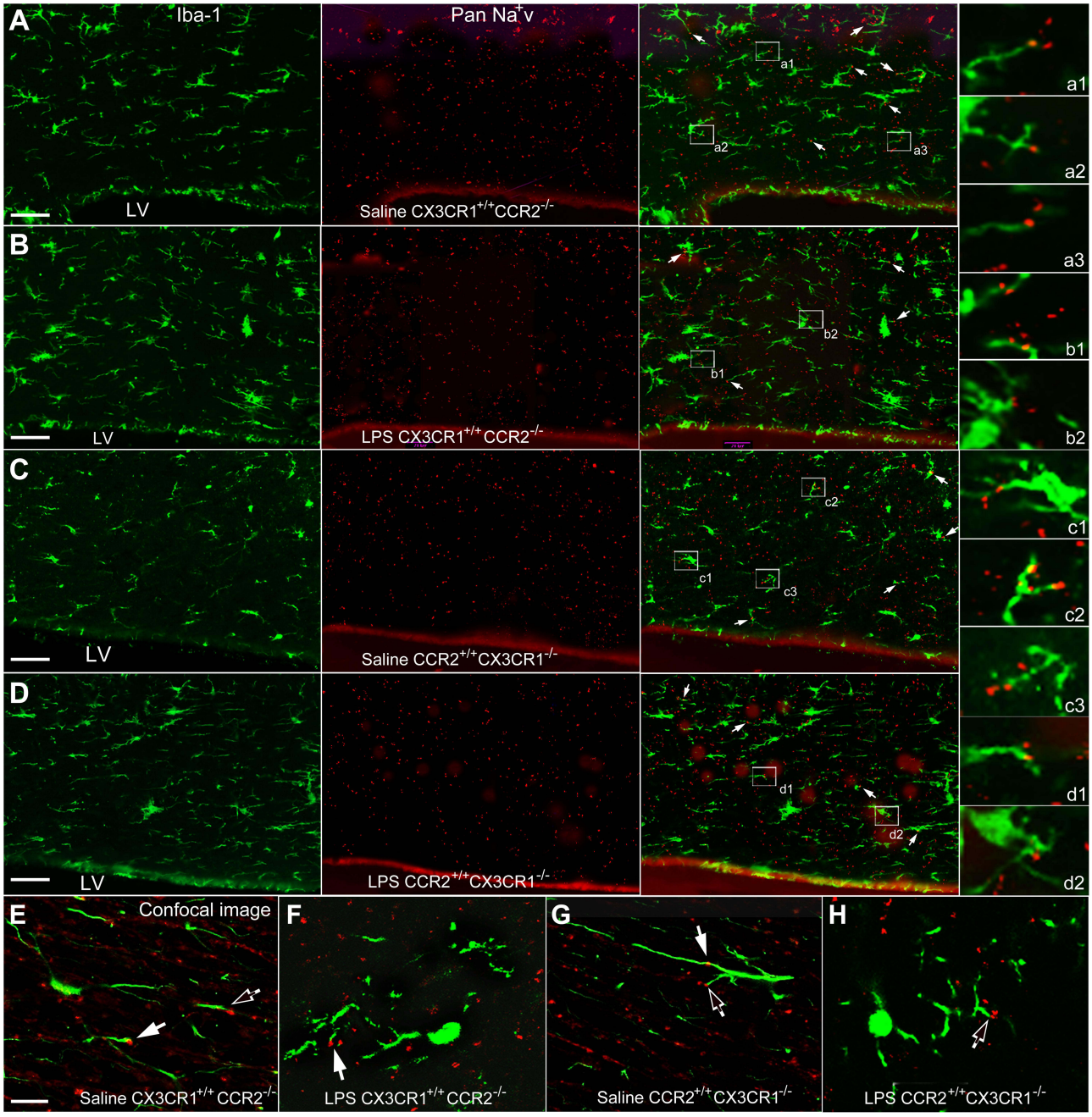

Figure 5 Contact between Iba-1 and Pan Na^+v labeling in the two transgenic mice. (**A** and **C**), contact or close apposition between Iba-1 and Pan Na^+v labeling (arrows and frame areas) in the CC of saline injected $CX3CR1^{+/+}CCR2^{-/-}$ and $CCR2^{+/+}CX3CR1^{-/-}$ mice, respectively. (a1–a3 and c1–c3) amplified images from the frame areas in (**A** and **C**) (**B** and **D**) and (b1, b2, d1 and d2) showing these contact or close apposition in the LPS injected littermates. (**E–H**) confocal microscopic verification for contact (solid arrows) or close apposition (empty arrows) between Iba-1 and Pan Na^+v labeling. Scale bars are 20 μm in (**A–D**) and 10 μm at (**E–H**).

Discussion

An intriguing finding, which was not previously reported according to our broad literature search, is that CX3CR1 knockout clearly impeded the animal's ability to explore novel objects, since the time and ratio of reaching novel objects vs total exploration was significantly higher in naïve WT mice than in normal $CCR2^{+/+}CX3CR1^{-/-}$ mice (see Figure 1Ai and Bi). In addition, the absence of CX3CR1 obstructed the animal's spatial cognition because the ratio of correct alternation during the Y-maze test was approximately significantly lower in normal $CCR2^{+/+}CX3CR1^{-/-}$ mice than in naïve WT mice (see Figure 1Ci). Reasonably, people prefer to believe that the observed subnormal cognitive behavior stems from a disorder of

https://doi.org/10.2147/JIR.S513429

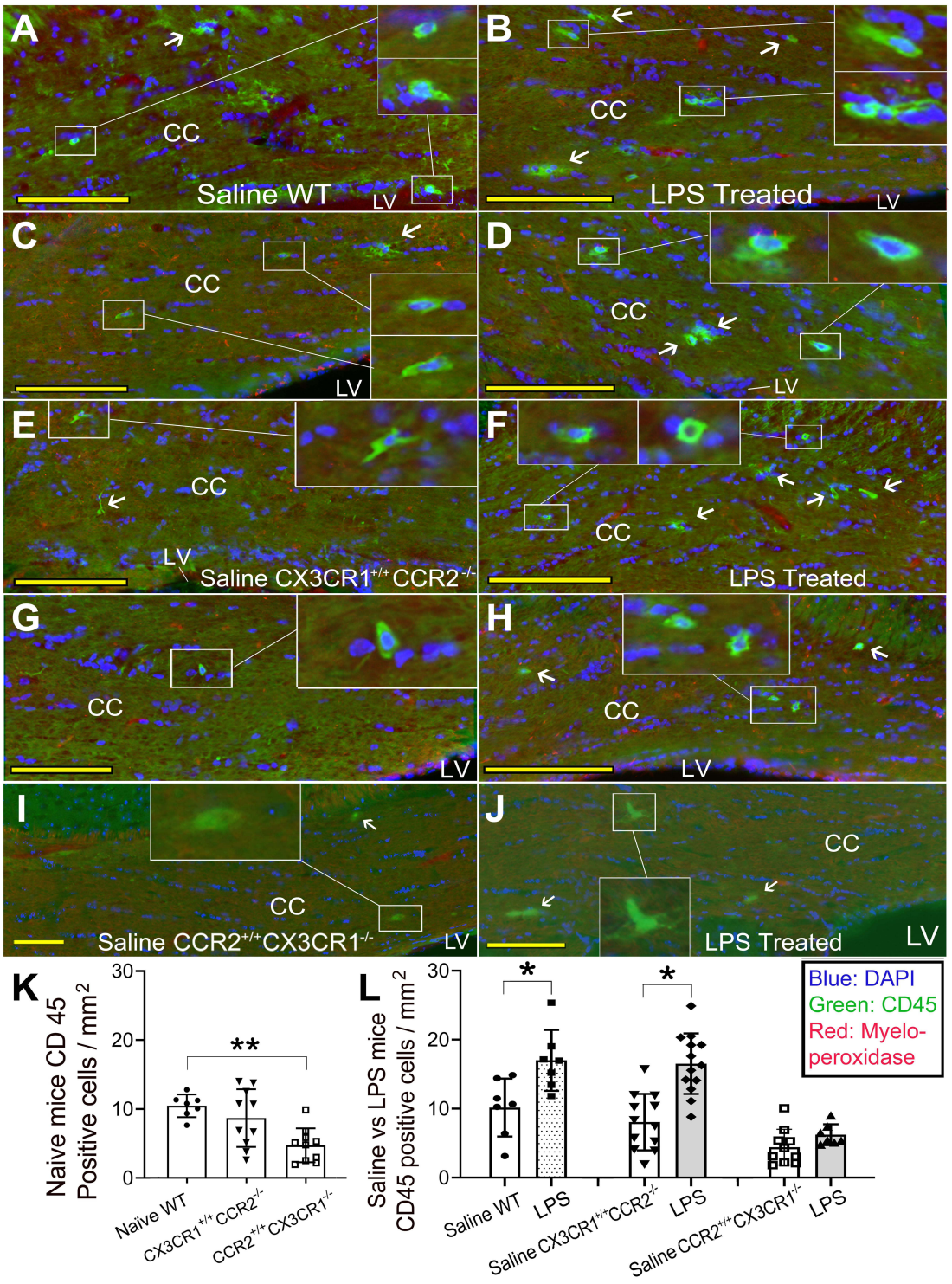

Figure 6 CD 45 labeled infiltrating immune cells in the CC of WT and two transgenic mice. (**A, C, E, G** and **I**) CD45 positive cells (arrows, frame areas and insets) in the CC of saline injected WT (**A** and **C**), CX3CR1$^{+/+}$CCR2$^{-/-}$ (**E** and **G**) and CCR2$^{+/+}$ CX3CR1$^{-/-}$ (**I**) mice. The CD45 labeled infiltrating cells were devoid of pseudopodia and MPO staining, and generally about 15–20 µm diameter along the long axis. Some lymphocyte-size cells were round-shaped with about 10 µm or less in diameter (arrows in **A, C, E** and **I**). (**B, D, F, H** and **J**) CD45 labeled cells in the CC of LPS treated ones (arrows, frame areas and insets). Clusters of CD45 labeled cells were sometimes visualized (inset in **B**, opposite arrows in **D** and **F**). A ramified CD45 positive, macrophage like cell was viewed in the CC of LPS treated CCR2$^{+/+}$CX3CR1$^{-/-}$ mice (inset in **J**). Dark red MPO like immunoreactivity appeared to be situated mostly in blood vessel like structures, and co-localized with neither CD45 labeling nor DAPI marked nucleus. (**K**) CD45 positive cells in the CC of naïve WT mice (n = 3) were significantly more than that in normal CCR2$^{+/+}$CX3CR1$^{-/-}$ ($F_{2, 24} = 7.92$, $p < 0.01$, n = 4) mice. (**L**) systemic LPS significantly increased CD45 positive cells in the CC of WT ($F_{7, 62} = 32.10$, $p < 0.05$, n = 3) and CX3CR1$^{+/+}$CCR2$^{-/-}$ mice ($F_{7, 62} = 32.10$, $p < 0.05$, n = 4), but not in CCR2$^{+/+}$CX3CR1$^{-/-}$ mice (n = 4), in comparison of their saline injected littermates. The marks of "*" and "**" represent $p < 0.05$ and $p < 0.01$, respectively. Scale bars are 100 µm in (**A–H**) and are 50 µm in (**I** and **J**).

brain regions that dominate learning and memory, such as the hippocampus. Indeed, CX3CL1 and CX3CR1 knockout results in hippocampal dysfunction indicated by anomalous long-term potentiation (LTP), poor motor learning, and Morris water maze deficits.[6–8] Additionally, we revealed that CX3CR1 knockout yielded a more evident decline in the WM tract CAP than CCR2 deletion, in comparison to WT mice (see Figure 2B and C). Hence, CX3CR1 knockout not only induces hippocampal dysfunction, but also disrupts the conductive function of the CC WM tract. The latter should have an additional impact on relevant abnormal cognitive behavior. Previous studies have suggested that the hippocampal neuronal network is disordered because CX3CR1 knockout abolishes the synapsis pruning function of microglia, leading to cognitive impairment.[6–8] Correspondingly, we examined the effect of CX3CR1 knockout on microglia-node contact, which may modulate WM tract conductive function, as aforementioned.[22–24] Statistically, the number of microglia-node contacts or close appositions was significantly fewer in CX3CR1 deficiency mice than in WT mice (see Figures 4 and 5). This is probably due to the lower microglia density in the CC (see Figure 3A–O) of the two transgenic mice, because Pan Na^+v intensity was virtually identical between WT and the two transgenic mice (see Figure 4E). Hence, CX3CR1 knockout interrupts both the microglia-neuron interaction in the hippocampus, especially the synapsis pruning function, and microglia-node communication in the CC WM tract. Thus, the current study demonstrated reduced capabilities to explore novel objects and novel trails, anomalous conductive function, lower microglia density and disrupted microglia-node communication in the CC WM tract simultaneously in the same animals, *ie* in the CX3CR1 deficiency mice.

Considering the pro-inflammatory roles of CX3CL1-CX3CR1 and CCL2-CCR2,[3,4] we would like to know what happens in the WM tract during systemic inflammation if CX3CR1 or CCR2 are absent. Following systemic LPS, the ratio of exploring new objects vs total exploration was significantly decreased in WT and CX3CR1 equipped mice, but not in CX3CR1 deficiency ones (see Figure 1Aii and Bii). In addition, the ratio of correct alternation during the Y-maze test was nearly significantly reduced by LPS challenge in WT and CX3CR1 positive mice, but not in CX3CR1 deficiency mice (see Figure 1Cii). Coincidently, the I/O curve plotted from the myelinated fiber's CAP was clearly downshifted by systemic LPS in CX3CR1 positive mice, with a significantly decreased CAP amplitude at 0.40–0.50 mA stimulation points (see Figure 2D). The I/O curve of unmyelinated CC fibers in CX3CR1 equipped mice was also downshifted by LPS treatment, with a significantly lower CAP amplitude at the 0.50 mA intensity point (see Figure 2H). These results were unexpected because it has been documented that the CCL2-CCR2 axis plays a major pro-inflammatory roles in many pathological procedures.[37] However, we realized that this outcome was fairly consistent after we examined microglia-node contact or their close apposition, since systemic LPS significantly reduced the number of these contacts and/or appositions in the CC of WT and CX3CR1 expressed mice, but not in CX3CR1 knock-out mice (see Figure 4H). Our confocal microscopic data revealed that some of the "contacts" under a conventional microscope were "close appositions" with a 0.5 ~ 1.5 μm gap. We believe that this distance is close enough for microglial pseudopodia to modulate the cation balance around nodes[22,23] and possibly influences saltatory conduction. Without CX3CR1 mediated microglia activity, LPS treatment did not appear to significantly impact microglia-node contact and/or their close apposition to reduce the WM tract CAP and saltatory conduction, resulting in defective cognitive behavior. Nonetheless, we did not exclude LPS induced hippocampal malfunction, and ensued cognition impairment.[6,7] Systemic inflammation insults both the hippocampus and CC WM tract, as reported in a previous study,[36] in which systemic LPS induced functional changes in both the hippocampus and CC WM, reflected by abnormal LTP and decreased CAP. LTP recovered sooner after acute inflammation, but subnormal CAP persisted for a relatively longer time,[36] suggesting a faster reaction and recovery of the hippocampus during inflammatory insult in comparison with CC WM. This might explain why WM tract abnormalities are more prevalent in chronic systemic inflammation.[12–14]

Apart from the effect of CX3CR1 knockout on cognitive performance and WM tract function in healthy and LPS-challenged mice, CCL2-CCR2 signaling has been reported to mediate cognitive impairment by reducing hippocampal neurogenesis.[9] The authors observed a correlation between reduced neurogenesis, defective cognition, and increased hippocampal neuronal CCL2 without mentioning CCR2 cellular resources. The prerequisites for these positive results are chronic pain,[9] or actually the chronic inflammation. Two types of circulating monocytes have been identified: $CCR2^{high}$/$CX3CR1^{low}$ and $CX3CR1^{high}$/$CCR2^{low}$ monocytes. The former generally guides monocytes into inflamed tissues, whereas the latter commonly mediates immune cell infiltration into non-inflamed tissues.[3,4] Thus, in the present study, we scanned the infiltration of circulating immune cells into the CC WM using anti-CD45, a common leukocyte

antigen,[38,39] to quantify the infiltrated immune cells in CX3CR1$^{+/+}$/CCR2$^{-/-}$ or CCR2$^{+/+}$/CX3CR1$^{-/-}$ mice. The primary antibody used in this study was specific for mouse CD45, reacted with most murine isoforms,[36] and immunostained monocytes and lymphocytes (see https://www.thermofisher.com/antibody/product/CD45-Antibody-clone-30-F11-Monoclonal/14-0451-82). This result was not as ideal as expected: the number of CD45 labeled cells in the CC WM of CX3CR1$^{+/+}$CCR2$^{-/-}$ mice was significantly increased by LPS challenge but was not significantly elevated in CCR2$^{+/+}$CX3CR1$^{-/-}$ mice (see Figure 6L). It was appeared the CCR2^{high} circulating monocytes may not be primarily recruited by inflamed CC WM.[4,37,40] This number should be significantly elevated by LPS treatment in CCR2$^{+/+}$CX3CR1$^{-/-}$ mice, if CCR2^{high} monocytes are predominantly recruited. Nonetheless, a line of studies had shown that CX3CR1^{high} myeloid cells or monocyte/macrophage are inflammatory mediators in a multiple scleroses and a peripheral nerves neuropathy model.[41,42] The infiltrated monocytes/macrophages in the spinal cord WM were CX3CR1^{high}, and CX3CR1 antagonists significantly attenuated paralysis and inhibited relapse.[41] Monocyte/macrophage infiltration in the peripheral nervous bundle was predominantly the CX3CR1^{high} subset in a peripheral neuropathy model.[42] To our knowledge, this is the first study to demonstrate that CX3CR1^{high} circulating immune cells are the major infiltrating cells in the CC WM tract of normal and LPS-challenged mice (see Figure 6K and L).

Conclusion

1) Whole data from the current study inferred that the CX3CL1-CX3CR1 axis plays a major role in modulating microglia-node contact and their close apposition in the CC WM, in maintaining WM tract conductive function, and in proper cognitive performance. 2) In circumstances of systemic endotoxin and associated neuroinflammation, broken this axis seemed to dominate disrupted microglia-node communication and concomitant WM tract dysfunction, and was involved in cognition impairment. 3) The aforementioned sequences may be achieved primarily through CX3CL1-CX3CR1 mediated microglia activities and collaterally via recruitment of CX3CR1^{high} circulating immune cells into the CC WM, which exacerbates microglia-node miscommunication-induced WM tract dysfunction and cognitive impairment.

Data Sharing Statement

All data relevant to the article are available upon request.

Acknowledgments

We thank Dr. Laura Maile, Department of Anesthesiology, University of Cincinnati College of Medicine for her critical reading and English improvement. We appreciate the assistance of our colleagues in The Electrophysiological Lab of The Fifth Medical Center of PLA General Hospital, China. This paper has been uploaded to Research Square as a preprint: [https://www.researchsquare.com/article/rs-3626477/v1].

Author Contributions

All authors made a significant contribution to the work reported, whether that is in the conception, study design, execution, acquisition of data, analysis and interpretation, or in all these areas; took part in drafting, revising or critically reviewing the article; gave final approval of the version to be published; have agreed on the journal to which the article has been submitted; and agree to be accountable for all aspects of the work.

Funding

This study was supported by the National Natural Science Foundation of China [No. 81974168], author GAO-F received this funding. This study was partially supported by the Research grant of Key Laboratory of Molecular Biological Targeted Therapy of the Ministry of Education (Huazhong University of Science and Technology) [No. 2024SWBS016], and an open foundation of Hubei Key Laboratory of Biological Targeted Therapy [No. 202413].

Disclosure

The authors declare that they have no conflicts of interest to disclose for this work.

References

1. Du Y, Zhang Q, Zhang X, et al. Correlation between inflammatory biomarkers, cognitive function and glycemic and lipid profiles in patients with type 2 diabetes mellitus: a systematic review and meta-analysis. *Clin Biochem*. 2023;121-122:110683. doi:10.1016/j.clinbiochem.2023.110683
2. Misiak B, Beszlej JA, Kotowicz K, et al. Cytokine alterations and cognitive impairment in major depressive disorder: from putative mechanisms to novel treatment targets. *Prog Neuropsychopharmacol Biol Psychiatry*. 2018;80(Pt C):177–188. doi:10.1016/j.pnpbp.2017.04.021
3. Spiteri AG, Wishart CL, Pamphlett R, et al. Microglia and monocytes in inflammatory CNS disease: integrating phenotype and function. *Acta Neuropathol*. 2022;143(2):179–224. doi:10.1007/s00401-021-02384-2
4. Shi C, Pamer EG. Monocyte recruitment during infection and inflammation. *Nat Rev Immunol*. 2011;11(11):762–774. doi:10.1038/nri3070
5. Stuart MJ, Baune BT. Chemokines and chemokine receptors in mood disorders, schizophrenia, and cognitive impairment: a systematic review of biomarker studies. *Neurosci Biobehav Rev*. 2014;42:93–115. doi:10.1016/j.neubiorev.2014.02.001
6. Wang L, Ling H, He H, et al. Dysfunctional synaptic pruning by microglia correlates with cognitive impairment in sleep-deprived mice: involvement of CX3CR1 signaling. *Neurobiol Stress*. 2023;25:100553. doi:10.1016/j.ynstr.2023.100553
7. Rogers JT, Morganti JM, Bachstetter AD, et al. CX3CR1 deficiency leads to impairment of hippocampal cognitive function and synaptic plasticity. *J Neurosci*. 2011;31(45):16241–16250. doi:10.1523/JNEUROSCI.3667-11.2011
8. Méndez-Salcido FA, Torres-Flores MI, Ordaz B, et al. Abnormal innate and learned behavior induced by neuron-microglia miscommunication is related to CA3 reconfiguration. *Glia*. 2022;70(9):1630–1651. doi:10.1002/glia.24185
9. Chen L, Qin Q, Huang P, et al. Chronic pain accelerates cognitive impairment by reducing hippocampal neurogenesis may via CCL2/CCR2 signaling in APP/PS1 mice. *Brain Res Bull*. 2023;205:110801. doi:10.1016/j.brainresbull.2023.110801
10. Filley CM, Fields RD. White matter and cognition: making the connection. *J Neurophysiol*. 2016;116(5):2093–2104. doi:10.1152/jn.00221.2016
11. Catani M, Dell'acqua F, Bizzi A, et al. Beyond cortical localization in clinico-anatomical correlation. *Cortex*. 2012;48(10):1262–1287. doi:10.1016/j.cortex.2012.07.001
12. Samara A, Murphy T, Strain J, et al. Neuroinflammation and white matter alterations in obesity assessed by diffusion basis spectrum imaging. *Front Hum Neurosci*. 2019;13:464. doi:10.3389/fnhum.2019.00464
13. Bian R, Zhang Y, Yang Y, et al. White matter integrity disruptions correlate with cognitive impairments in asthma. *J Magn Reson Imaging*. 2018. doi:10.1002/jmri.25946
14. Lu Y, Zhou S, Fan C, et al. Higher inflammation and cerebral white matter injury associated with cognitive deficit in asthmatic patients with depression. *J Asthma*. 2022;59(2):288–296. doi:10.1080/02770903.2020.1853155
15. Inaba T, Yamashiro K, Kurita N, et al. Microbial lipopolysaccharide-induced inflammation contributes to cognitive impairment and white matter lesion progression in diet-induced obese mice with chronic cerebral hypoperfusion. *CNS Neurosci Ther*. 2023;1(Suppl 1):200–212. doi:10.1111/cns.14301
16. Huang P, Chen X, Hu X, et al. Experimentally induced sepsis causes extensive hypomyelination in the prefrontal cortex and hippocampus in neonatal rats. *Neuromolecular Med*. 2020;22(3):420–436. doi:10.1007/s12017-020-08602-6
17. Healy D, Murray C, McAdams C, et al. Susceptibility to acute cognitive dysfunction in aged mice is underpinned by reduced white matter integrity and microgliosis. *Commun Biol*. 2024;7(1):105. doi:10.1038/s42003-023-05662-9
18. Sanchez-Molina P, Almolda B, Benseny-Cases N, et al. Specific microglial phagocytic phenotype and decrease of lipid oxidation in white matter areas during aging: implications of different microenvironments. *Neurobiol Aging*. 2021;105:280–295. doi:10.1016/j.neurobiolaging.2021.03.015
19. Zhang J, Boska M, Zheng Y, et al. Minocycline attenuation of rat corpus callosum abnormality mediated by low-dose lipopolysaccharide-induced microglia activation. *J Neuroinflammation*. 2021;18(1):100. doi:10.1186/s12974-021-02142-x
20. Yang X, Zhang JD, Duan L, et al. Microglia activation mediated by toll-like receptor-4 impairs brain white matter tracts in rats. *J Biomed Res*. 2018;32(2):136–144. doi:10.7555/JBR.32.20170033
21. Waxman SG, Ritchie JM. Molecular dissection of the myelinated axon. *Ann Neurol*. 1993;33(2):121–136. doi:10.1002/ana.410330202
22. Zhang J, Yang X, Zhou Y, et al. Direct contacts of microglia on myelin sheath and Ranvier's node in the corpus callosum in rats. *J Biomed Res*. 2019;33(3):192–200. doi:10.7555/JBR.32.20180019
23. Ronzano R, Roux T, Thetiot M, et al. Microglia-neuron interaction at nodes of Ranvier depends on neuronal activity through potassium release and contributes to remyelination. *Nat Commun*. 2021;12(1):5219. doi:10.1038/s41467-021-25486-7
24. Wu W, He S, Wu J, et al. Long-term in vivo imaging of mouse spinal cord through an optically cleared intervertebral window. *Nat Commun*. 2022;13(1):1959. doi:10.1038/s41467-022-29496-x
25. Chattopadhyay N, Ye C, Yamaguchi T, et al. The extracellular calcium-sensing receptor is expressed in rat microglia and modulates an outward K+ channel. *J Neurochem*. 1999;72(5):1915–1922. doi:10.1046/j.1471-4159.1999.0721915.x
26. Eyo UB, Gu N, De S, et al. Modulation of microglial process convergence toward neuronal dendrites by extracellular calcium. *J Neurosci*. 2015;35(6):2417–2422. doi:10.1523/JNEUROSCI.3279-14.2015
27. Saederup N, Cardona AE, Croft K, et al. Selective chemokine receptor usage by central nervous system myeloid cells in CCR2-red fluorescent protein knock-in mice. *PLoS One*. 2010;5(10):e13693. doi:10.1371/journal.pone.0013693
28. Jung S, Aliberti J, Graemmel P, et al. Analysis of fractalkine receptor CX(3)CR1 function by targeted deletion and green fluorescent protein reporter gene insertion. *Mol Cell Biol*. 2000;20(11):4106–4114. doi:10.1128/MCB.20.11.4106-4114.2000
29. Xiao L, Li L, Huang J, et al. Salidroside attenuates lipopolysaccharide-induced neuroinflammation and cognitive impairment in septic encephalopathy mice. *Int Immunopharmacol*. 2023;117:109975. doi:10.1016/j.intimp.2023.109975
30. Ennaceur A, Delacour J. A new one-trial test for neurobiological studies of memory in rats. 1: behavioral data. *Behav Brain Res*. 1988;31(1):47–59. doi:10.1016/0166-4328(88)90157-x
31. Yu K, Zhou H, Chen Z, et al. Mechanism of cognitive impairment and white matter damage in the MK-801 mice model of schizophrenia treated with quetiapine. *Behav Brain Res*. 2024;461:114838. doi:10.1016/j.bbr.2023.114838
32. Kraeuter AK, Guest PC, Sarnyai Z. The Y-maze for assessment of spatial working and reference memory in mice. In: PC G, editor. *Pre-Clinical Models, Techniques and Protocols*. New York: Humana Press; 2019:105–112.
33. Donnelly DJ, Gensel JC, Ankeny DP, et al. An efficient and reproducible method for quantifying macrophages in different experimental models of central nervous system pathology. *J Neurosci Methods*. 2009;181(1):36–44. doi:10.1016/j.jneumeth.2009.04.010

34. Crawford DK, Mangiardi M, Tiwari-Woodruff SK. Assaying the functional effects of demyelination and remyelination: revisiting field potential recordings. *J Neurosci Methods*. 2009;182(1):25–33. doi:10.1016/j.jneumeth.2009.05.013
35. Reeves TM, Phillips LL, Povlishock JT. Myelinated and unmyelinated axons of the corpus callosum differ in vulnerability and functional recovery following traumatic brain injury. *Exp Neurol*. 2005;196(1):126–137. doi:10.1016/j.expneurol.2005.07.014
36. Zhang J, Li A, Song Z. Systemic LPS resulted in a transient hippocampus malfunction but a prolonged corpus callosum injury. *BMC Anesthesiol*. 2017;17(1):105. doi:10.1186/s12871-017-0396-1
37. Mysore V, Tahir S, Furuhashi K, et al. Monocytes transition to macrophages within the inflamed vasculature via monocyte CCR2 and endothelial TNFR2. *J Exp Med*. 2022;219(5). doi:10.1084/jem.20210562
38. Virts E, Barritt D, Siden E, et al. Murine mast cells and monocytes express distinctive sets of CD45 isoforms. *Mol Immunol*. 1997;34(16–17):1191–1197. doi:10.1016/s0161-5890(97)00142-9
39. Grindem CB. Blood cell markers. *Vet Clin North Am Small Anim Pract*. 1996;26(5):1043–1064. doi:10.1016/s0195-5616(96)50055-0
40. Geissmann F, Jung S, Littman DR. Blood monocytes consist of two principal subsets with distinct migratory properties. *Immunity*. 2003;19 (1):71–82. doi:10.1016/s1074-7613(03)00174-2
41. Ridderstad Wollberg A, Ericsson-Dahlstrand A, Jureus A, et al. Pharmacological inhibition of the chemokine receptor CX3CR1 attenuates disease in a chronic-relapsing rat model for multiple sclerosis. *Proc Natl Acad Sci U S A*. 2014;111(14):5409–5414. doi:10.1073/pnas.1316510111
42. Oladiran O, Shi XQ, Fournier S, et al. CX3CR1 but not CCR2 expression is required for the development of autoimmune peripheral neuropathy in mice. *Front Immunol*. 2021;12:720733. doi:10.3389/fimmu.2021.720733